Materials Research, Vol. 12, No. 2, 181-190, 2009

Electrospinning and Characterization of Polyamide 66 Nanofibers With Different Molecular Weights

Lilia Muller Guerrini[a], *Marcia Cristina Branciforti*[a], *Thomas Canova*[b], *Rosario Elida Suman Bretas*[a]*

[a]*Department of Materials Engineering, Federal University of São Carlos, 13565-905 São Carlos - SP, Brazil*
[b]*Rhodia Têxtil, Santo André - SP, Brazil*

Received: December 23, 2008; Revised: May 8, 2009

Polyamide 66 (PA66) nanofibers of different molecular weights were obtained by electrospinning of formic acid solutions. An ionic salt, NaCl, was also added to the solutions to increase the conductivity. PA66 concentrations between 15-17 wt.(%)/v and electrical fields between 2.0 and 2.5 kV/cm were the best conditions to produce the smallest nanofibers; however, the addition of NaCl increased the fibers average diameters.

The characterization of the fibers was done by scanning electron microscopy (SEM), differential scanning calorimetry (DSC), wide angle X rays diffraction (WAXD) and Fourier Transformed Infrared (FTIR). As the molecular weight decreased, the nanofibers average diameters also decreased; however, critical number average and weight average molecular weights were necessary for electrospinning. As the amounts of carboxyl terminal groups (CTG) increased, the nanofibers average diameters decreased; however, above CTG's critical values of 8.7×10^{-5} mol.g^{-1} no electrospinning was possible. The addition of ionic salt increased the electrical conductivity of the solutions and increased the nanofibers' average diameters. By DSC, residual solvent in all the electrospun mats was found; two melting endotherms, one between 248 and 258 °C and the other one between 258 and 267 °C, depending on the sample were also observed. These endotherms were attributed to the melting, re-crystallization and re-melting of the PA66 α-phase. The nanofibers had low % of crystallinity compared to a textile fiber. By WAXS and FTIR, confirmation of the presence of α-phase crystals, of small dimensions and highly imperfect and of a very small amount of β and γ-phases crystals in the nanofibers structure was obtained.

Keywords: *polyamide 66, electrospinning, nanofiber, characterization*

1. Introduction

Electrospinning of polymer solutions has been extensively used in the last years to produce polymeric fibers of nano-dimensions[1-6]. New companies based on this process, like eSpin Technologies, Nanotechnics and Kato Tech emerged in the last years while companies like Donaldson and Freudenberg have been using electrospun fibers for the last two decades[7]. In the electrospinning process, the polymeric solution is put in a capillary tube or syringe and a metallic electrode, connected to a grounded high voltage supply is immersed in the polymeric solution. An electrical tension is applied and when the electrostatic forces overcome the solution's surface tension, the hemispherical surface of the capillary's drop (Taylor's cone) elongates and an electrically charged jet of polymeric solution is generated. During the jet's trajectory to the collector, the solvent evaporates; thus solid nanofibers are formed and collected in the form of non-woven mats on the metallic collector. The variables of this process are many: solutions concentration (which determines the solutions viscosity), solvent type, applied electrical field, ionic salts addition (which can increase the solution's electrical conductivity), flow rate, temperature and others.

The molecular weight, the distribution of molecular weight and branching of the polymer have also influence on the electrospinning because can interfere on the solvent's evaporation rate, crystallization kinetics and solutions viscosity. In the case of poly-condensation polymers like PA66, the amount of terminal carboxylic and amines groups should also have an effect on the process.

The electrospinning of PA66 has been done by other authors[8,9]; Martin et al.[8] electrospun solutions of PA66 in formic acid with 10 and 16 wt.(%)/v. They obtained non-woven mats with 0.06-2.80 μm of diameter. Tsai and Chen[9] also electrospun solutions of PA66 in formic acid. They obtained nanofibers with average diameter of 78 nm. However, none of these works analyzed the influence of the PA66 molecular weight and terminal carboxylic and amines groups on the electrospinning.

On the other hand, polyamide 6 (PA6) has been more extensively studied. Hag-Yong et al.[10] electrospun solutions of PA 6 in sulfuric acid with 15 wt.(%)/v, obtaining fibers with average diameters lower than 500 nm. Ryu et al.[11] also electrospun solutions of PA6 in formic acid at 15 and 30 wt.(%)/v obtaining fibers with average diameters between 90 and 500 nm. Dersh et al.[12] measured the Herman's orientation function of electrospun fibers from formic acid solutions and concluded that γ crystals with high orientation along the flow direction formed the PA6 structure. Stephens et al.[13] electrospun PA6 solutions in hexa-isofluoropropanol and found that the PA6 crystalline structure changed from α-phase to γ-phase. Suphapol et al.[14,15] electrospun solutions of PA6/formic acid with different molecular weights; they found that the higher the molecular weight, the higher the nanofibers average diameters.

The addition of an ionic salt sometimes increases the electrical conductivity of the solution. As Reneker et al.[3] pointed out, in an uncharged ionic solution, there is the same number of positive and negative ions in each volume element. When an external electrical

*e-mail: bretas@power.ufscar.br

field is applied to the solution, the positive and negative ions move toward the negative and positive electrodes, respectively. The difference in the number of positive and negative ions in a particular region (for example near the electrodes) is called the excess charge. The excess charge produces an electrical field that extends for large distances. When an ionic salt is added, it dissociates into equal numbers of positive and negative ions, which increase the electrical conductivity of the solution by increasing the number of ions per unit volume, but do not increase the excess charge. Thus, for each polymeric solution there is a suitable ionic salt which will increase the electrical conductivity depending on the initial excess charge. For example, studies of the effect of the addition of NaCl in poly (vinyl alcohol) electrospun solutions[16] have shown that the fibers average diameters decrease when the ionic salt is added; however, other studies in electrospun solutions of PA6/formic acid/NaCl[14] have observed that the fibers' average diameter increase when the salt is added. Even no effect on the fibers average diameters[17] has been found.

Thus, in this work, the influence of the molecular weight and amount of terminal carboxylic and amines groups on the average diameters of electrospun nanofibers of PA66 will be investigated. The influence of the addition of an ionic salt on these fibers average diameters will also be studied.

2. Experimental

2.1. Materials

Two different molecular weights PA66 from Rhodia® were used, sample B and sample C. Sample B was post-condensed to obtain higher molecular weights, by two different routes in a vacuum oven: one at 140 °C, during 4 hours (sample A) and the other at 150 °C, during 24 hours (sample D). Sample C, suitable for the production of textiles, was also post-condensed by two different routes: one, before melt spinning, under vacuum, at 150 °C, during 24 hours (sample R) and the other during the liquid synthesis before melt spinning for 5 minutes (sample F)[18].

The solvent used for the electrospinning solutions was formic acid (85%, from Synth®) with density of 1.22 g.mL^{-1} at 20 °C, molar mass of 46.03 g.mol^{-1}, boiling point of 101 °C and melting point of 8.6 °C. Two conductive solutions (samples DS and RS) were prepared by the addition of NaCl (1 wt.(%)/v). Table 1 describes the nomenclature of the samples.

2.2. Polyamide 66 characterization

The amount of carboxyl terminal groups, CTG, was determined by titration using benzyl alcohol, phenolphthalein and methanol as solvents of the polyamide at 200 °C and a solution (0.1 N) of potassium hydroxide/glycol as titration agents. The CTG in g.mol^{-1} was calculated using the following Equation 1:

$$CTG = \frac{(v - v_0)\ f_c}{m} \quad (1)$$

where v = consumed volume of titration agent during the polyamide titration (l); v_0 = consumed volume of titration agent in the white (without polyamide) titration (l); M = molarity of the titrate (mol.L^{-1}); f_c = correction factor of the titrate (calculated in a daily basis to correct possible errors in the titrate preparation); and m = sample mass (g).

The correction factor f_c was determined by weighting a standard sample of pure potassium hydrogen phthalate. This standard sample was titrated with potassium hydroxide/glycol (0.1 N) solution. The correction factor was calculated using the following Equation 2:

$$f_c = 1000\ m_{fs} / (V\ N\ 204.23) \quad (2)$$

where m_{fs} = mass of potassium hydrogen phthalate (g); V = volume of titrate (l); N = normality of the titrate; and 204.23 = equivalent-gram of potassium hydrogen phthalate.

The amount of amines terminal groups, ATG, was determined by potentiometer titration using phenol and tri-(hydroxy-methyl) amino methane as solvents of the polyamide at 40 °C and HCl as titration agent, in a potentiometer from Mettler Toledo®, model DL-50 with a Pt electrode. The ATG, in g.mol^{-1}, was calculated using Equation 3:

$$ATG = \frac{(v - v_0)Mf_c}{m} \quad (3)$$

The amount of humidity in the polyamide was determined by loss weight at 105 °C during 30 minutes in a vacuum oven.

The number average molecular weight, M_n, was determined from Equation 4:

$$M_n = \frac{2 \times 10^6}{\sum (ATG + CTG + 8)} \quad (4)$$

where: 8 = number of end-chain groups that are neither amines or carboxyl groups[19,20].

2.3. Solutions preparation and characterization

The polyamide 66/formic acid solutions were prepared at 40 °C, under agitation. The polyamide concentrations in the formic acid were 10, 15, 17 and 20 wt.(%)/v. Solutions with 1 wt.(%)/v of NaCl were also prepared.

The solutions electrical conductivities were measured in a conductimeter from Digimed®, model DM-31, with a Pt electrode. The solutions' surface tension was measured by the du Nöy method using a tension meter from Krüss, model K6, with a Pt ring. The shear viscosity of the solutions at low shear rates was measured in an ARES rheometer, from Rheometrics Scientific, using Couette geometry with a gap of 2 mm between the cylinders, under nitrogen atmosphere, at 25 °C.

Table 1. Nomenclature of the polyamide 66 samples.

Samples description	Post-condensation conditions	Name of the sample and solution
Polyamide 66 (pellets)	-	B
Polyamide 66 (pellets)	Vacuum, 140 °C, 4 hours	A
Polyamide 66 (pellets)	Vacuum, 150 °C, 24 hours	D
Polyamide 66 , textile (pellets)	-	C
Polyamide 66, textile (pellets)	Vacuum, 150 °C, 24 hours	R
Polyamide 66 (fibers)	During synthesis	F
Sample D + 1 wt.(%)/v NaCl (solution)	-	DS
Sample R + 1 wt.(%)/v NaCl (solution)	-	RS

2.4. Solutions electrospinning

The electrospinning equipment was composed of a glass syringe (20 mL), a cylindrical collector and a high voltage supply, as shown in Figure 1. The syringe had Hamilton type stainless steel needles. The syringe electrode was a Cu thread sustained by a Cu peg. The collector was composed of a poly (vinyl chloride) tube (20 cm diameter), in which two wood disks were fixed at the ends. One of the wood disks was grounded, while the other was coupled to a motor, from Tekno®, model MRT910, with a velocity regulator, also from Tekno, model CVET2002. To measure the amount of rpm, a tachometer from Minipa®, model MDT-2238A was used. The collector was covered with an aluminum foil. The high voltage supply was from Bertan, model 210-30R.

The solutions electrospinning was done at room temperature and without room humidity control.

Tables 2 to 5 show the electrospinning conditions in which each sample was processed. Sample B was also electrospun, but no nanofibers were formed at any condition.

2.5. Nanofibers characterization

2.5.1. Scanning Electron Microscopy (SEM)

The electrospun nanofibers were deposited on a double-face carbon adhesive and glued to the sample holder; silver paint was then added at the mats borders. The sample was gold sputtered and analyzed using two scanning electron microscopes: one from Zeiss®, Model DSM940, operating at 15 kV and the other from Phillips®, model XL30 FEG, operating at 30 kV. The number average diameter of the nanofibers and its distribution were calculated using the Image Pro-Plus software, in the Zeiss® micrographs; 100-120 fibers average diameters were measured.

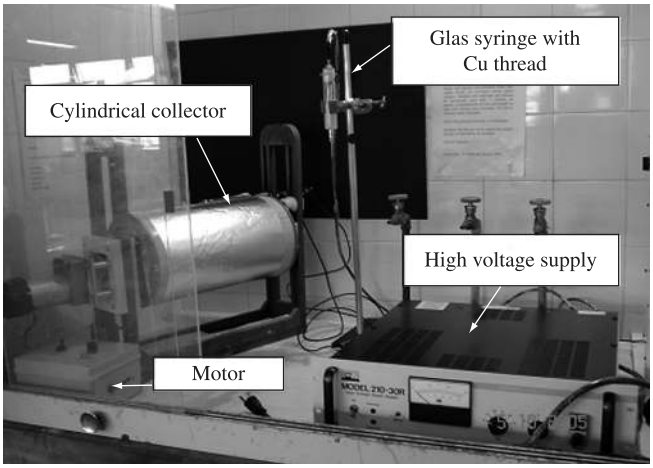

Figure 1. Electrospinning set-up used in this work.

Table 2. Electrospinning conditions of sample A.

Sample	Solution concentration (wt.(%)/v)	Electrical field (kV/cm)	Number average diameter (nm)
A3	10	2.5	-
A4	10	2.9	-
A5	15	2.0	131
A6	15	2.5	153
A13	17	2.0	148
A14	17	2.5	143
A2	17	2.5	155
A8	20	2.5	176

2.5.2. Differential Scanning Calorimetry (DSC)

The glass transition temperature (Tg), the melting temperature (T_m), the amount of residual solvent ($X_{r,s}$) and the apparent amount of crystallinity of the nanofibers were measured by DSC, in a TA Instruments equipment, model Q100. The nanofibers were heated between 30 and 300 °C at 10 °C/min. The amount of crystallinity was calculated as the ratio between the melting enthalpy of the sample and the melting enthalpy of a theoretical 100% crystalline sample (ΔHf^o_m). For the polyamide 66, $\Delta Hf^o_m = 206\ J.g^{-1}$ [21].

Table 3. Electrospinning conditions of sample D.

Sample	Solution concentration (wt.(%)/v)	Electrical field (kV/cm)	Number average diameter (nm)
D1	15	1.5	150
D2	15	2.0	148
D3	15	2.5	140
D4	17	1.5	153
D5	17	2.0	158
D6	17	2.5	161
D7	20	1.5	198
D8	20	2.0	180
D9	20	2.5	188
DS6	17	2.5	174

Table 4. Electrospinning conditions of sample R.

Sample	Solution concentration (wt.(%)/v)	Electrical field (kV/cm)	Number average diameter (nm)
R1	15	1.5	150
R2	15	2.0	133
R3	15	2.5	117
R4	17	1.5	155
R5	17	2.0	136
R6	17	2.5	147
R7	20	1.5	185
R8	20	2.0	171
R9	20	2.5	163
RS1	15	1.5	163
RS2	15	2.0	152
RS3	15	2.5	152
RS4	17	1.5	158
RS5	17	2.0	184
RS6	17	2.5	166
RS7	20	1.5	182
RS8	20	2.0	179
RS9	20	2.5	176

Table 5. Electrospinning conditions of sample F.

Sample	Solution concentration (wt.(%)/v)	Electrical field (kV/cm)	Number average diameter (nm)
F2	10	1.5	-
F3	10	2.0	-
F8	15	1.0	164
F9	15	1.3	173
F5	15	1.5	150
F10	15	1.7	172
F6	15	2.0	140
F7	15	2.5	166
F21	15	3.0	-
F15	17	1.0	176
F16	17	1.3	167
F14	17	1.5	165
F17	17	1.7	163
F12	17	2.0	170
F13	17	2.5	140
F18	17	3.0	182
F19	17	4.0	190
F20	17	5.0	187

2.5.3. Wide angle X ray diffraction (WAXD) and Fourier Transform Infrared (FTIR)

To analyze the type of crystalline phases in the nanofibers, WAXD and FTIR experiments were done. The WAXD measurements were made in a diffractometer from Siemens® model D5005, operating with CuKα radiation, Ni filter, at 40 kV and 40 mA. The diffractograms were decomposed using the Origin 7.0 software with a Gaussian approximation. For the infrared analyses, mats of the nanofibers were pile up to form a "film". A FTIR equipment from Perkin Elmer® model Spectrum® 1000 was used, between 400 to 4,000 cm^{-1}, in the transmission mode, with 4 cm^{-1} of resolution.

3. Results and Discussion

3.1. Polyamide 66 and solutions characterization

Table 6 shows the molecular weights, the ATG and the CTG of the different samples. As the molecular weight of the polyamide 66 increased as a consequence of post-condensation, the amount of amines and carboxyl terminal groups decreased, as expected. Sample B had the lowest molecular weight, while sample F had the highest molecular weight.

Table 7 shows the zero shear viscosity, η_o, the surface tension τ and the electrical conductivity K of some of the solutions. The η_o of all the solutions increased with the increase in PA 66 concentrations, as expected. The values of surface tension and electrical conductivity of solutions A, D and R were similar to the values of PA6/ formic acid solutions. Li et al.[22], for example, found surface tension values between 41 and 42 mN/m and electrical conductivities values between 4.6 and 4.3 mS/cm for PA6/formic acid solutions, with concentrations of 15 and 20 wt.(%)/v. Suphapol et al.[15] also found surface tension values between 44 and 42 mN/m for the same type of solutions. The surface tension of solutions F was lower than of the other solutions, probably due to the lower amount of amines and carboxyl groups (lower interactions).

Table 6. Properties of the polyamide 66.

Sample	M_n ($g.mol^{-1}$)	M_w ($g.mol^{-1}$)	ATG $_x10^{-5}$ ($mol.g^{-1}$)	CTG $_x10^{-5}$ ($mol.g^{-1}$)
B	13879	27759	4.78	8.83
A	14970	29940	4.02	8.54
D	17621	35242	2.80	7.76
R	16750	33501	2.43	8.71
F	19194	38388	1.70	7.92

Table 7. Zero shear viscosity, η_0, surface tension, τ, and electrical conductivity, K, of the polyamide 66 solutions.

Sample	C (wt.(%)/v)	η_0 (Pa.s)	τ (mN/m) 25 °C	K(mS/cm) 25 °C
Formic acid	-	0.00095	45	2.6
B	10	0.06050	45	4.3
A	10	0.06195	-	-
	15	0.2369	44	-
	17	0.2811	44	-
	20	0.5759	45	-
D	15	0.2066	-	-
	17	0.4385	45	4.5
	20	0.7439	44	4.9
R	15	0.2595	44	4.6
	17	0.4343	45	4.6
	20	0.7945	45	4.5
F	10	0.4112	37	4.4
	15	0.6247	37	4.7
	17	1.2340	37	4.7
DS	17	0.4724	43	7.0
	20	0.9314	44	7.4
RS	15	0.2480	41	8.4
	17	0.5344	41	8.2
	20	0.7577	42	7.9

The addition of 1wt.%/v NaCl increased the electrical conductivity of the solutions, as expected, but did not have any effect on the surface tension (Table 7). Solutions DS (7.0-7.4 mS/cm) and RS (7.9-8.4 mS/cm) almost doubled their conductivities by the addition of the salt, while the D and R solutions without salt had electrical conductivities between 4.5 and 4.9 and 4.5 and 4.6 mS/cm, respectively.

3.2. Nanofibers characterization

Some of the Phillips® scanning electron micrographs of the nanofibers mats are shown in Figures 2, 3, 4, 5, 6 and 7, together with the distribution of nanofibers diameters calculated from the Zeiss® micrographs, as described in the experimental section. Tables 2 to 5 also show the number-average fiber diameter of all the electrospun samples. SEM micrographs of solution B are not shown, because, as said before, the electrospinning of that solution did not produce nanofibers, only drops.

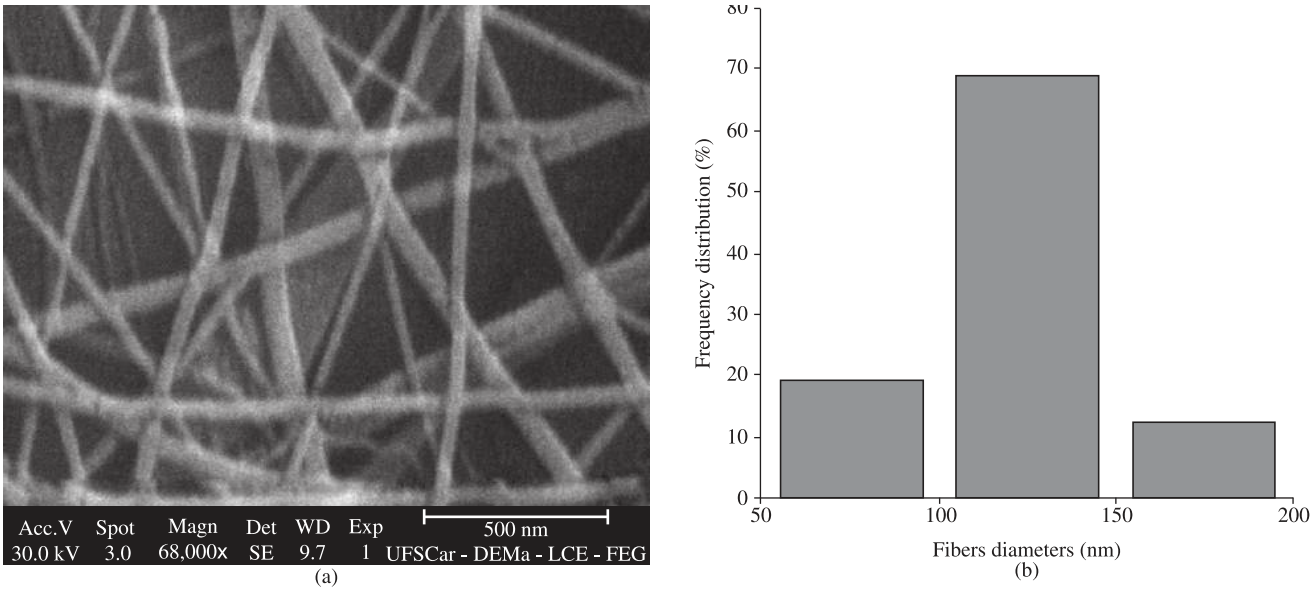

Figure 2. a) Micrograph of sample A5 (Phillips® SEM); and b) diameter distribution (Zeiss® SEM).

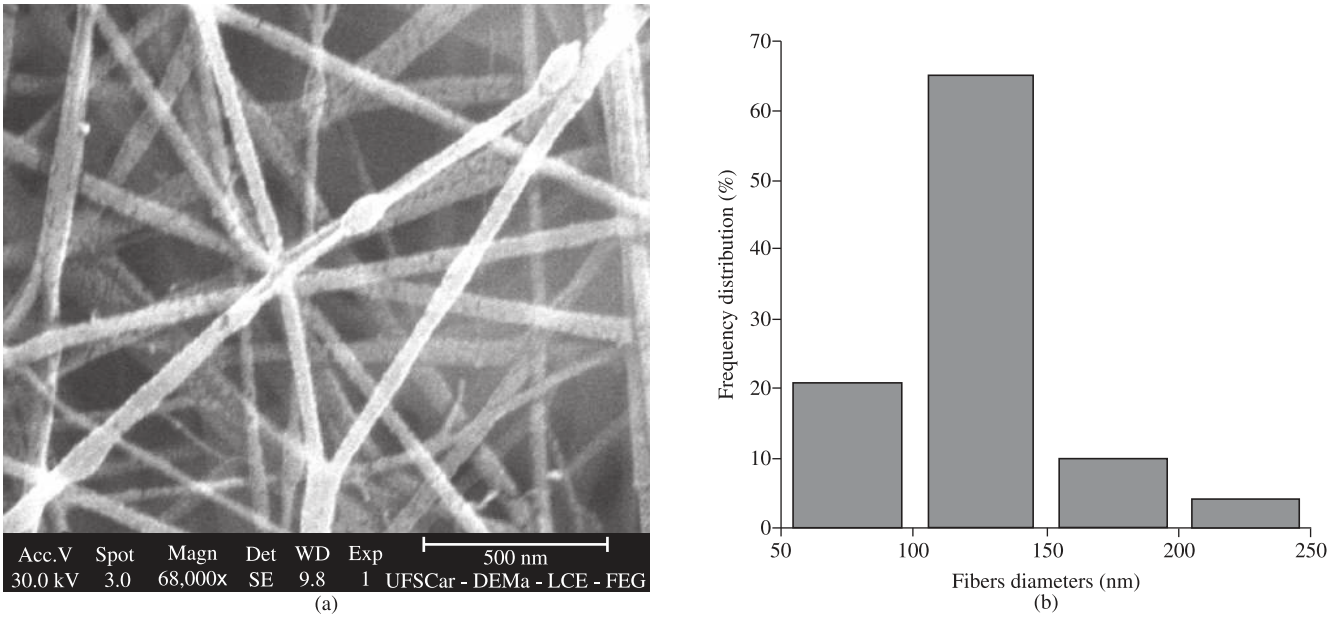

Figure 3. a) Micrograph of sample D3 (Phillips® SEM); and b) diameter distribution (Zeiss® SEM).

The smallest diameter (117 nm) was obtained from the electrospinning of sample R, followed by sample A (131 nm), while samples D and F produced the largest fibers (140 nm). Therefore, as a rule, as the molecular weight increased, the nanofibers average diameters also increased; also, the higher the amount of carboxyl terminal groups, however, the lower the nanofibers average diameters. This last effect can be credited to the formation of hydrogen bonds that would facilitate the alignment of the macromolecules during the spinning.

The smallest average diameters of samples A were obtained at A5 electrospinning conditions (15 wt.(%)/v, 2.0 kV/cm); D3 conditions (15 wt.(%)/v, 2.5 kV/cm) produced the smallest average diameters of samples D. R3 electrospinning conditions (15 wt.(%)/v, 2.5 kV/cm) also produced the smallest average diameters of samples R. F6 (15 wt.(%)/v, 2.0 kV/cm) and F13 (17 wt.(%)/v, 2.5 kV/cm) conditions produced the smallest average diameters of samples F. In this last case, however, the F6 condition produced 79% of fibers with average diameter of 125 nm, while the F13 condition produced 47% of nanofibers with average diameter of 125 nm.

Therefore, PA66 concentrations in formic acid between 15-17 wt.%/v and electrical fields between 2.0 and 2.5 kV/cm were the best electrospinning conditions to produce the smallest nanofibers.

The addition of NaCl to sample R increased the nanofibers' average diameters; the smallest diameter after the salt addition was obtained from the electrospinning of sample RS2 (15 wt.(%)/v,

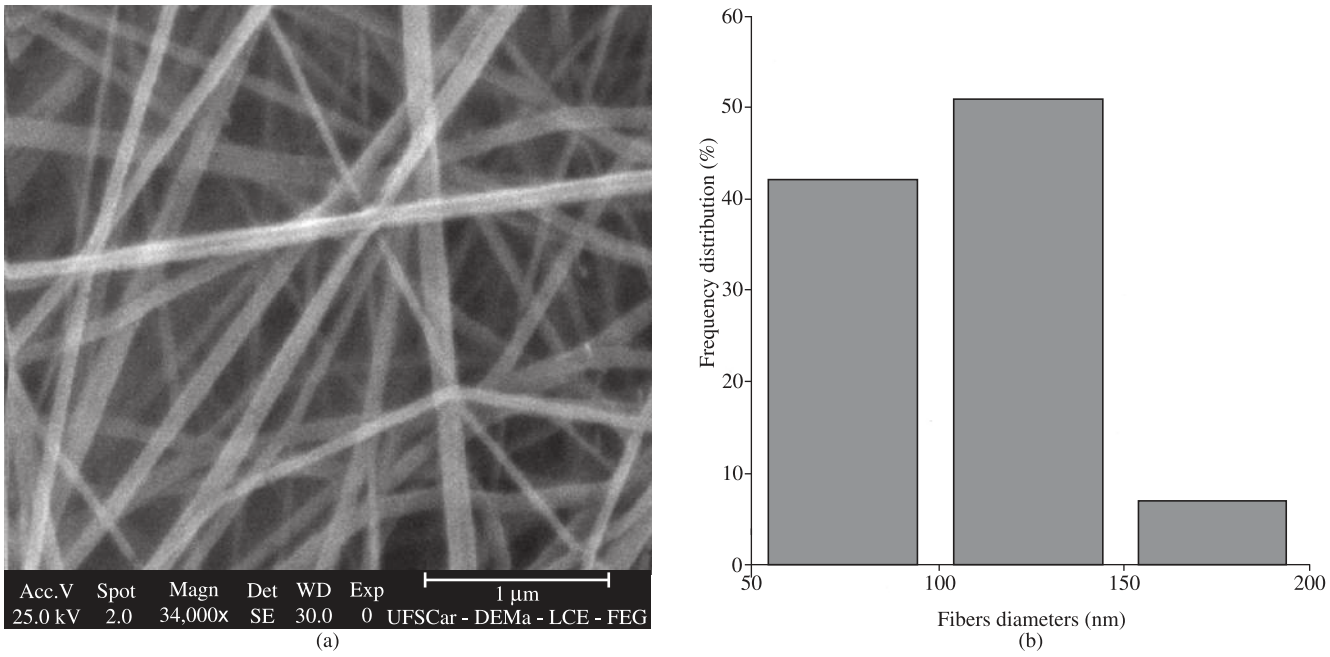

Figure 4. a) Micrograph of sample R3 (Phillips® SEM); and b) diameter distribution (Zeiss® SEM).

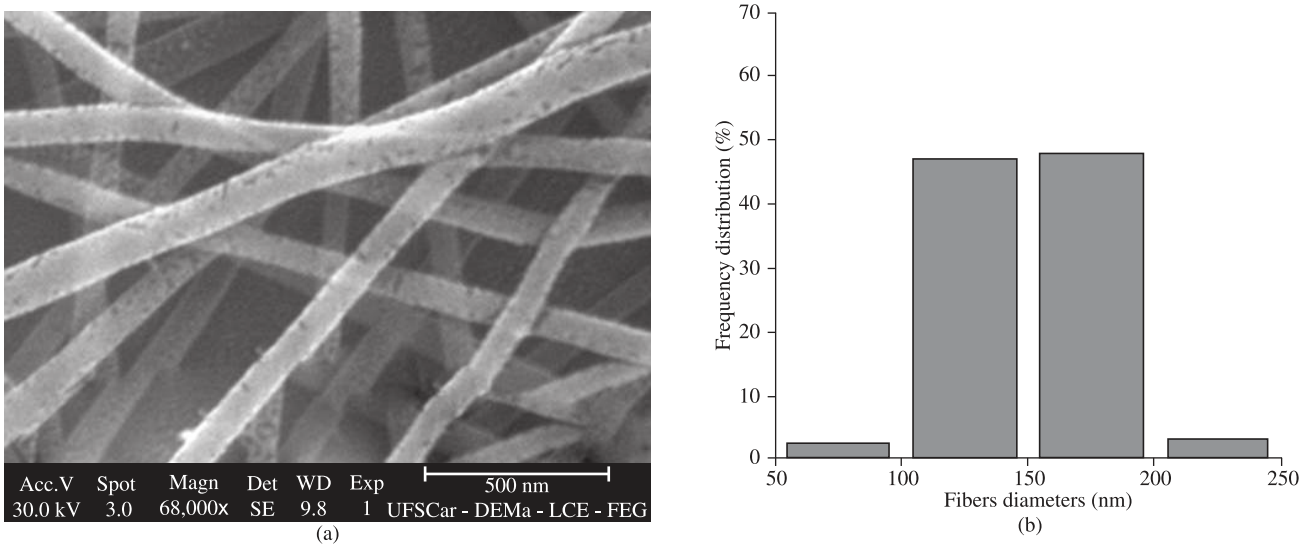

Figure 5. a) Micrograph of sample F 13 (Phillips® SEM); and b) diameter distribution (Zeiss® SEM).

2.0 kV/cm). The same average diameter increase was observed with the addition of the salt to sample D; in this case, only condition DS6 (17 wt.(%)/v, 2.5 kV/cm) produced nanofibers. Thus, as a rule, the addition of NaCl increased the nanofibers' average diameters.

To analyze the influence of concentration of the PA 66 solution, an electrical field of 2.5 kV/cm was chosen for comparison. Regarding samples A, D and R, it is observed that as the PA66 concentration in the solution increased, the nanofibers' average diameter also increased. However, the opposite behavior is observed with sample F: the higher the PA66 concentration in the solution, the lower the nanofibers average diameters. As said before, Sample F had the lowest surface tension but the higher M_n and M_w of all the samples; this combination allowed a quicker jet formation and higher amount of entanglements, producing fibers with lower average diameters.

Evaluating these results and the properties of the polyamide 66 (Table 6) it can be observed that the nanofibers average diameters is low when the polyamide 66 molecular weight decreases; however, critical molecular weights of Mn ≥ 14,970 $g.mol^{-1}$ and Mw ≥ 29,940 $g.mol^{-1}$ were necessary for electrospinning. In addition, the nanofibers average diameter was low as the amount of carboxyl terminal groups (CTG) increased; however, above a critical CTG ≥ 8.7×10^{-5} $mol.g^{-1}$ no electrospinning was possible.

Finally, to analyze the influence of the electrical field, a solution concentration of 15 wt.(%)/v was chosen. Samples D and R behaved as expected: the higher the applied electrical field, the lower the

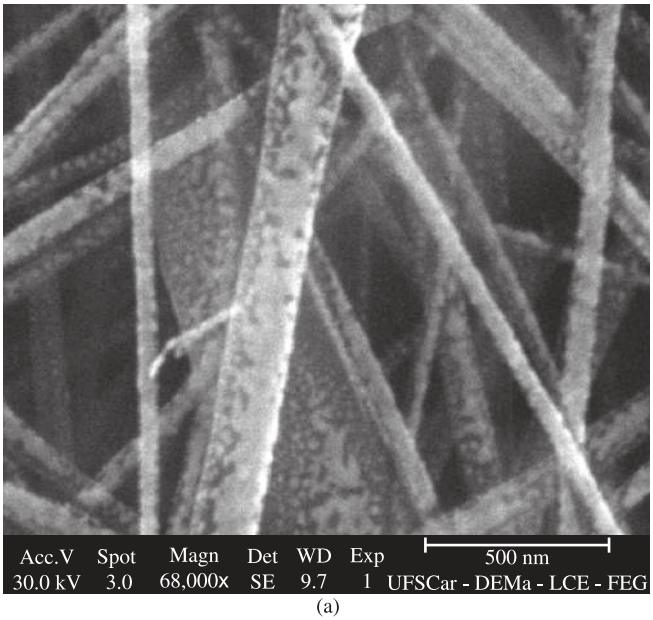

(a)

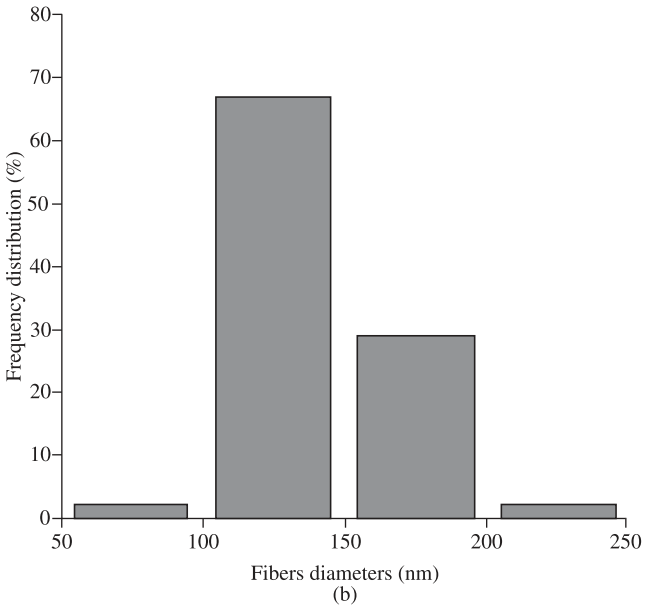

(b)

Figure 6. a) Micrograph of sample RS2 (Phillips® SEM); and b) diameter distribution (Zeiss® SEM).

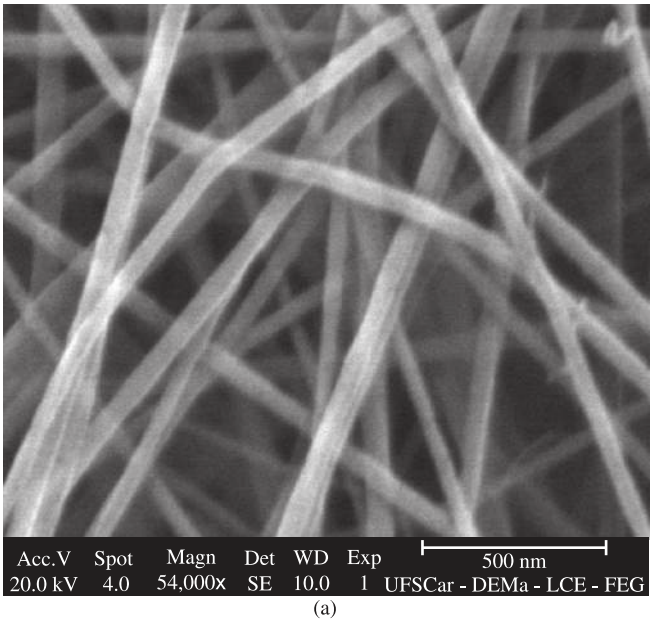

(a)

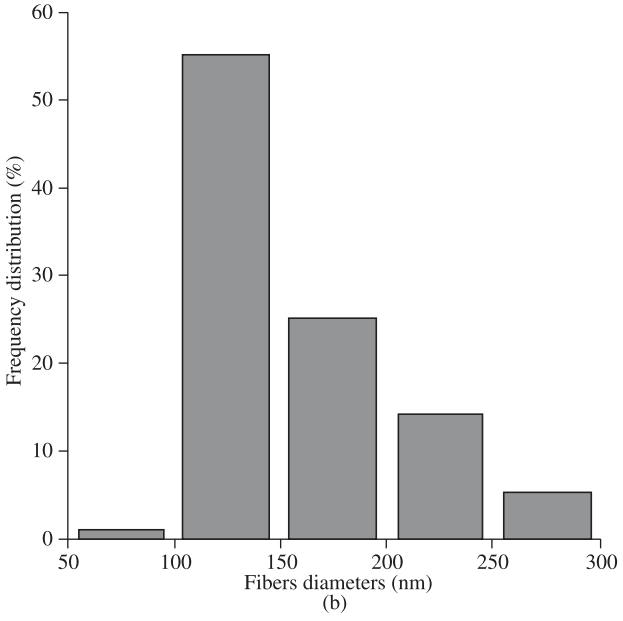

(b)

Figure 7. a) Micrograph of sample DS6 (Phillips® SEM); and b) diameter distribution (Zeiss® SEM).

nanofibers average diameter. On the other hand, sample A had an opposite behavior: the higher the electrical field, the higher the average diameter. Sample F did not suffered influence of the increase of the electrical field, probably because it had the lowest surface tension of all the solutions.

Because the smallest nanofibers were obtained from sample R, only these mats were characterized by DSC. Figure 8 shows the heating runs of those mats, while Table 8 shows the main thermal transitions.

PA66 has a Tg between 45-65 °C. During the heating run, the Tg was not observed in the samples. Instead a large endothermic peak, ΔH_v (between 31 and 130 °C, accounted for solvent evaporation) was observed. That is, after the electrospinning residual solvent remained in the mats. The percentage of residual solvent $X_{r,s,}$ was calculated from Equation 5:

$$X_{r.s} = \frac{m}{m_T} \times 100 \quad (5)$$

where: m = vaporized formic acid mass (Kg); m_T = DSC sample mass (Kg).

The vaporized formic acid mass was calculated from the DSC enthalpy of vaporization ΔH_v = m (cΔT + L), where ΔT = end vaporization temperature - initial vaporization temperature, c = specific

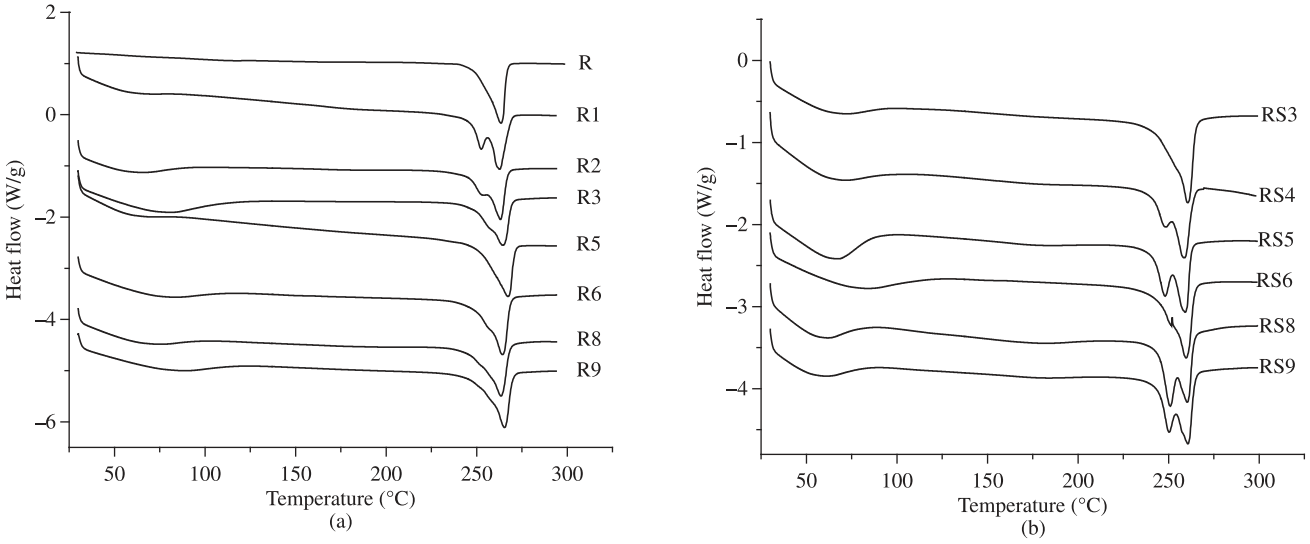

Figure 8. DSC heating run of sample R: a) R mats without salt; and b) R mats with salt.

Table 8. Main thermal transitions, amount of residual solvent, $X_{r,s}$, and crystallinity of sample R nanofibers.

Sample	T_g (°C)	ΔH_v (J.g^{-1})	$X_{r,s}$(%)	Tm_1 (°C)	ΔH_1 (J.g^{-1})	Tm_2 (°C)	ΔH_2 (J.g^{-1})	Crystallinity (%)
R	-	-	-	-	-	263.3	77.4	38
R1	N.O	46.9	2.2	252.3	31.7	262.4	55.1	15
R2	N.O	62.7	2.5	253.7	40.1	263.7	37.1	20
R3	N.O	148.0	5.0	257.2	51.9	265.0	22.8	25
R5	N.O	60.8	2.8	N.O	-	267.6	73.9	-
R6	N.O	104.0	4.2	257.1	61.5	264.1	25.0	30
R8	N.O	69.4	2.6	252.8	56.6	263.3	24.6	28
R9	N.O	112.2	3.4	258.5	54.2	265.9	27.2	26
RS3	N.O	63.7	2.5	255.0	61.1	260.7	21.9	30
RS4	N.O	77.5	3.6	248.5	31.2	258.5	30.5	15
RS5	N.O	96.8	3.8	248.0	33.9	259.4	38.4	17
RS6	N.O	100.4	3.2	251.5	55.1	260.2	22.0	27
RS8	N.O	62.9	2.4	251.1	40.9	260.7	37.0	20
RS9	N.O	59.0	2.6	250.6	36.5	261.6	40.3	18

N.O = not observable.

heat capacity of the formic acid in the liquid state = 2169 J.kg^{-1} K and L = latent heat of vaporization of formic acid = 41.4 x 10^6 J.kg^{-1} [21].

The amount of residual solvent varied from 2.2 to 5.0% for the R mats without salt and from 2.4 to 3.8% for the R mats with salt.

Regarding the melting of the samples, it was observed that all samples had two melting endotherms: one between 248 and 258 °C, ΔH_1, and the other one between 258 and 267 °C, ΔH_2, depending on each sample. Because no cold crystallization was observed during the heating run, it was assumed that melting, re-crystallization and re-melting of the PA66 α-phase gave rise to these two endotherms. ΔH_1 was attributed to the melting of imperfect α-crystals, which re-crystallized into more perfect α-crystals; these last ones, by its turn, melted absorbing the heat ΔH_2. That is, electrospinning of PA 66 gave rise to the formation of imperfect α-crystals which melted between 248-258 °C.

Thus, the apparent % of crystallinity of the nanofibers was calculated as:

$$\% \text{ crystallinity} = (\Delta H_1/\Delta Hf^o_m) \times 100 \quad (6)$$

The apparent amount of crystallinity of both types of mats was between 15 and 30%. A textile PA66 fiber usually has around 40% of crystallinity[23]; that is, the nanofibers had low amount of crystallinity compared to a textile fiber.

The PA66 electrospinning occurred at room temperature; therefore, it would be expected that no crystallization would occur during the spinning. However, two factors could have triggered crystallization: the lowering of the Tg by the solvent and the easiness of alignment of the PA66 macromolecules to form strong intermolecular hydrogen bonds.

Figure 9 shows the diffractogram of sample R and one of the mats, R9. It can be observed that the crystal structure of sample R is predominantly composed of α-phase, with diffraction peaks at 2θ = 20.5 and 23.0°[24,25]. A diffraction peak at 12.9° is also observed, related to the diffraction of γ-phase, as already found by Sengupta et al.[24] in solutions of polyamide 66 with formic acid. On the other hand,

the mats diffraction is large and amorphous-like, and no distinction between the diffraction of the crystalline planes and the amorphous halo is possible, indicating that the mats crystals are small and imperfect, as also inferred from the DSC analysis.

Infrared analyses of the R samples were also done. Figure 10 shows the FTIR spectra of sample R and the R9 mat. Table 9 shows the main peaks found in both spectra. The α-phase is predominant in both samples (peaks at 2935 and 2934 cm^{-1}); however, β and γ-phases (1437 and 1432 cm^{-1}) are also observed, but in a very small concentration. The amorphous phase (922 and 1128-1136 cm^{-1}) was not observed, probably due to overlapping by the crystalline peaks. The presence of CO_2 (doublet at 2362 and 2336 cm^{-1}, weak peak at 667 cm^{-1}) and water vapor (~3400 and 1620 cm^{-1}) was also observed.

Therefore the FTIR analyses confirmed the presence of mainly α-phase and small amounts of β and γ-phases in the PA66 nanofibers, as also found by Li et al.[26] after electrospinning PA66 in tetrafluoroethylene, TFE.

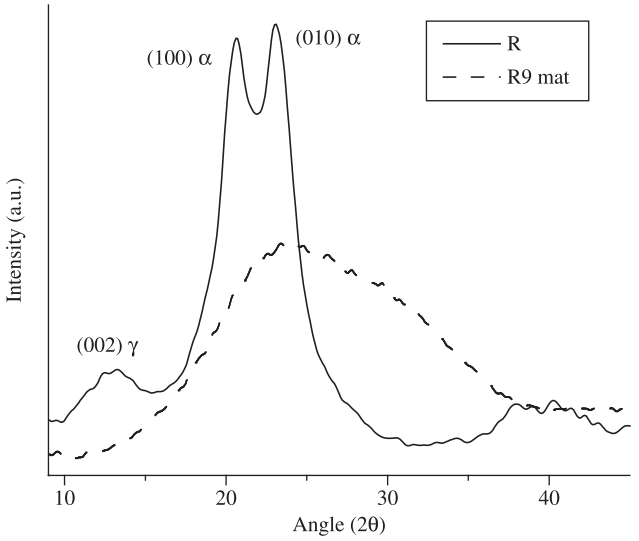

Figure 9. Diffractograms of sample R and R9 mat.

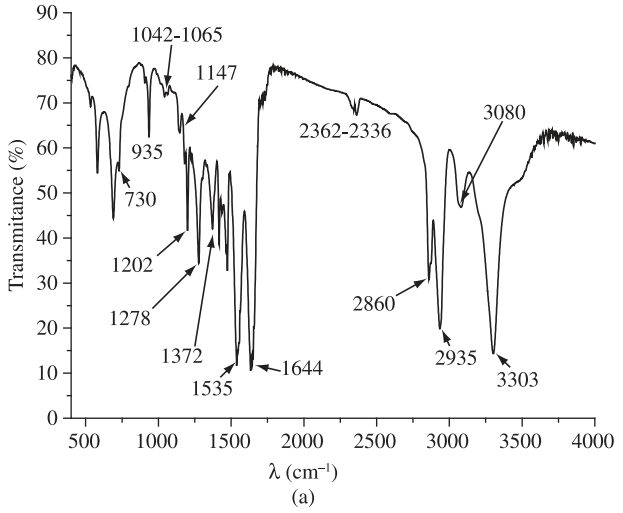

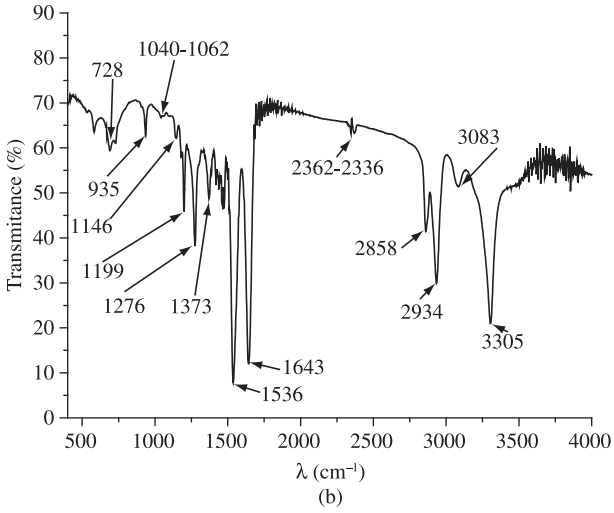

Figure 10. FTIR spectra of: a) sample R; and b) R9 mat.

4. Conclusions

The thermal and structural characterizations of the PA66 nanofibers allowed concluding that:

i) The lower the molecular weight, the lower the nanofibers average diameters; however, critical molecular weights of Mn ≥ 14,970 $g.mol^{-1}$ and Mw ≥ 29,940 $g.mol^{-1}$ were necessary for electrospinning.

ii) The higher the amount of carboxyl terminal groups, the lower the nanofibers average diameters; however, above critical CTG ≥ 8.7 x 10^{-5} $mol.g^{-1}$ no electrospinning was possible.

iii) Polyamide 66 concentrations in formic acid between 15-17 wt.%/v and electrical fields between 2.0 and 2.5 kV/cm were the best conditions to produce the smallest nanofibers.

iv) The addition of 1 wt.(%)/v NaCl doubled the electrical conductivity of the solutions and increased the nanofibers' average diameters.

v) The amount of residual solvent varied from 2.2 to 5.0% for the mats without salt and from 2.4 to 3.8% for the mats with salt; that is, all the mats contained residual solvent. All nanofibers had two melting endotherms: one between 248 and 258 °C and the other one between 258 and 267 °C, depending on the sample. Because no cold crystallization was observed during the DSC heating run, it was assumed that melting, re-crystallization and re-melting of the PA66 α-phase gave rise to these two endotherms. The nanofibers had low % of crystallinity compared to a textile fiber. By WAXD and FTIR, confirmation of the presence of α-phase crystals, of small dimensions and highly imperfect and of a very small amount of β and γ-phase crystals in the nanofibers structure was observed. That is, electrospinning of PA66 produced nanofibers with imperfect and small α-crystals which melted between 248-258 °C.

Acknowledgements

The authors would like to thank Prof. D. F. Petri for the tension surface measurements, L. R. B. Santos for the electrical conductivity measurements and Prof. R. Gregorio Filho for the high voltage power supply. This research was financially supported by CNPq and FAPESP.

Table 9. Main FTIR peaks observed in samples R and R9.

Peak (cm^{-1})	Characteristics	Sample R	Sample R9
721	Angular deformation out of plane, CH_2	730	728
932-937/940	Crystalline phase, amide axial deformation (C-C = O)	936	935
1033-1043 and 1063-1066	Triclinic structure, skeleton axial elongation (C-C)	1042, 1065 (weak)	1040, 1062 (weak)
1140-1146	Partially amorphous: angular deformation out of plane of carbonyl groups	1143	1146
1196-1202	Crystalline peak: symmetrical angular deformation out of plane, amide III.	1202	1199
~1220	Triclinic structure: angular deformation out of plane, (HN-C = O)	1220	1220
1300-1305	Triclinic structure: angular deformation out of plane, NH	1304 (weak)	1304 (weak)
~1370	CN axial deformation	1372	1373
~1440	γ-phase	1437 (weak)	1432 (weak)
1535-1555	C-N axial deformation and CO-N-H angular deformation, amide II	1535	1536
~ 1640	C = O axial deformation, amide I	1643	1644
~ 2858	CH_2 β-NH and γ-NH axial deformations	2860	2858
~ 2950	CH_2 α-NH axial deformation	2935	2934
~3080	N-H angular deformation in the plane	3080	3083
~3330-3060	Free N-H axial deformation	3305	3305

References

1. Huang ZM, Zhang YZ, Kotaki M, Ramakrishna S. A review on polymer nanofibers by electrospinning and their applications in nanocomposites. *Composites Science and Technology*. 2003; 63(15):2223-2253.
2. Ávila JPC. Alerta Tecnológico: Pedidos de Patentes sobre Nanotecnologia. Available from: <http://pt.espacenet.com>. Access in: 18/05/2009.
3. Reneker DH, Yarin AL. Bending instability of electrically charged liquid jets of polymer solutions in electrospinning. *Journal of Applied Physics*. 2000; 87(9):4531- 4547.
4. Mohan A. *Formation and characterization of electrospun nonwoven webs*. [Master thesis]. Raleigh: Faculty of North Caroline State University; 2002.
5. USPTO Patents and Trademarks Office Home. Available from: <www.uspto.gov>. Access in: 06/07/2007.
6. Doshi J, Reneker HD. Electrospinning process and application of electrospun fibers. *Journal of Applied and Polymer Science*. 1995; 35(2-3):151-160.
7. Ramakrishna S, Fujihara K, Teo WE, Yong T, Ma Z, Ramaseshan R. Review feature: electrospun nanofibers: solving global issues. *Materials Today*. 2006; 9(3):40-50.
8. Martin GE, Cockshott ID, Fildes FJT. Fibrilar lining for prosthetic device. US Patent 4, 044, 404, 1975.
9. Tsai PP, Chen W. Investigation of fiber, bulk, and surface properties of meltblown and electrospun polymeric fabrics. *International Nonwovens Journal*. 2004; 13(3):17-23.
10. Hag-Yong K, Myung-Seop G, Yoon-Ho J, Hyung-Jun K, Bong-Seok L. A process of preparation continuous filament composed of nanofiber. WO2004074559; 2004.
11. Ryu YJ, Kim HY, Lee KH, Park HC, Lee DR. Transport properties of electrospun nylon 6 nonwoven mats. *European Polymer Journal*. 2003; 39(9):1883-1889.
12. Dersch R, Liu T, Schaper AK, Greiner A, Wendorff JH. Electrospun nanofibers: internal structure and intrinsic orientation. *Journal of Polymer Science: Part A: Polymer Chemistry.* 2003; 41(4):545-553.
13. Stephens JS, Chase DB, Rabolt JF. Effect of electrospinning process on polymer crystallization chain conformation in nylon-6 and nylon-12. *Macromolecules*. 2004; 37(3):877-881.
14. Supaphol P, Mit-uppatham C, Nithitanakul M. Ultrafine electrospun polyamide-6 fibers: effect of emitting polarity on morphology and average fiber diameter. *Journal of Polymer Science: Part B: Polymer Physics*. 2005; 43(24):3699-3712.
15. Supaphol P, Mit-uppatham C, Nithitanakul M. Ultrafine electrospun polyamide-6 fibers: effect of solvent system and emmiting electrode polarity on morphology and fiber average diameter. *Macromolecular Materials and Engineering*. 2005; 290(9):933-942.
16. Zhang C, Yuan X, Wu L, Han Y, Sheng J. Study on morphology of electrospun poly(vinyl alcohol) mats. *European Polymer Journal*. 2005; 41(3):423-431.
17. Demir MM, Yigor I, Yilgor E, Erman B. Electrospinning of polyurethane fibers. *Polymer*. 2002; 43(11):3303-3309.
18. Guerrini LM, Canova T, Bretas RES. Procede dobtention dun produit contenant des nanofibres et produit contenant des nanofibres. Fr Patent 0700053; 2007.
19. Russell SA, Robertson DG, Lee JH, Ogunnaike BA. Control of Product Quality for Batch Nylon 6,6 Autoclaves. *Chemical Eng*ineering *Science.* 1998; 53(21): 3685-3702.
20. Waltz JE, Taylor GB. Determination of the molecular weight of nylon. *Journal of Applied and Polymer Science*. 1947; 19(1):448-450.
21. Lide DR. CRC Handbook of Chemistry and Physics. 88 ed. Taylor & Francis LLC, London: Editors Lide; 2007.
22. Li L, Bellan LM, Craighead HG, Frey MW. Formation and properties of nylon-6 and nylon-6/montmorillonite composite nanofibers. *Polymer.* 2006; 47(17):6208-6217.
23. Asprino TF. *Avaliação do comportamento de fadiga da interface entre cordonéis de poliamida 66 compatibilizados com resorcinol formaldeido/látex e compostos elastoméricos*. [Master thesis]. São Carlos: Federal University of São Carlos; 2007.
24. Sengupta R, Tikku VK, Somani AK, Chaki TK, Bhowimick AK. Electron beam irradiated polyamide-66 films-I: characterization by wide angle X-ray scattering and infrared spectroscopy. *Radiation Physics and Chemistry*. 2005; 72(5):625-633.
25. Muellerleile JT, Freeman JJ. Effect of solvent precipitation on the cystrallization behavior and morphology of nylon 66. *Journal of Applied Polymer Science*. 1994; 54(22):135-152.
26. Li Y, Huang Z, Lü Y. Electrospinning of nylon-66-6,10-10 terpolymer. *European Polymer Journal*. 2006; 42(7):1696-1704.